ECS Journal of Solid State Science and Technology, **2** (9) M28-M32 (2013)
2162-8769/2013/2(9)/M28/5/$31.00 © The Electrochemical Society

The Electrochemical Synthesis of the Graphite Intercalation Compounds Containing Tetra-n-alkylammonium Cations

Weekit Sirisaksoontorn and Michael M. Lerner[z]

Department of Chemistry, Oregon State University, Corvallis, Oregon 97331-4003, USA

The electrochemical intercalation of tetra-n-alkylammonium (TAA) cations into graphite is investigated using galvanostatic reduction and cyclic voltammetry in TAABr/ dimethylsulfoxide (DMSO) electrolytes. Structural and compositional analyzes by X-ray diffraction, thermogravimetric and elemental analyzes show that stable graphite intercalation compounds (GICs) are formed with highly-flattened TAA cation bilayers for $(C_5H_{11})_4N^+$, $(C_6H_{13})_4N^+$, $(C_7H_{15})_4N^+$, $(C_8H_{17})_4N^+$, with gallery expansions of 0.81 nm. $(C_4H_9)_4N^+$ forms a mixed-phase product including a stable GIC with monolayer TAA arrangement and a gallery expansion of 0.48 nm. The GICs with bilayer galleries incorporate 0.7–1.2 DMSO co-intercalate molecules per cation; the monolayer galleries contain relatively little DMSO. Although cyclic voltammetry shows that TAA cations smaller than $(C_4H_9)_4N^+$ do intercalate into graphite, they do not form stable GICs. The GICs obtained by galvanostatic reduction are compared to those prepared using chemical ion-exchange reactions. A surface passivation model is introduced to explain the relative stabilities of GICs formed with larger TAA cation intercalates.
 [DOI: 10.1149/2.042309jss]

Manuscript submitted May 31, 2013; revised manuscript received July 16, 2013. Published July 25, 2013.

Graphite exhibits a unique intercalation chemistry, and undergoes a wide range of reduction or oxidation reactions to form donor and acceptor-type graphite intercalation compounds (GICs), respectively.[1–3] Both chemical and electrochemical methods have been employed in the preparation of GICs.[4–7] Depending on the nature of the GICs and synthetic conditions, the intercalate ions (cations for donor-type, anions for acceptor-type GICs) may be accompanied by neutral co-intercalate molecules.[8] GICs display structural ordering perpendicular to the graphene sheet stacking direction; regular sequences of intercalate galleries and graphene layers arise in a phenomenon known as staging.[9,10] Stage-1 GICs have a single graphene sheet encased by intercalate galleries; stage-2 GICs have each bilayer of graphene sheets encased, and etc. Gallery expansion, Δd, is used to indicate the increased distance between graphene layer surfaces when separated by an intercalate gallery. Important applications of GICs to date include use as anodes in reversible lithium ion batteries,[11] as precursors to exfoliated graphite,[12–15] and in environmental oil absorption.[16]

Our group recently reported the first preparation of a series of symmetric or asymmetric tetra-n-alkylammonium GICs (TAAGICs) that were obtained via the quantitative displacement of the cationic complex, $Na(en)^+$, in $[Na(en)]C_{15}$ (square brackets indicate intercalates, x in C_x is the number of graphene carbons per negative charge, *en* is ethylenediamine) by TAA cations in an aprotic organic solvent such as dimethylsulfoxide (DMSO) or *N,N*-dimethylformamide (DMF).[17,18] Depending on the TAA cation employed, the TAAGIC products had Δd of either 0.47 nm or 0.8 nm, associated with the intercalation of either monolayers or bilayers of cations with highly-flattened conformations. These same gallery dimensions were obtained over the wide range of TAA cation diameters, from about 0.4–0.5 nm for $(C_4H_9)_4N^+$ to ≈1.4 nm in $(C_8H_{17})N^+$. The monolayer arrangement was only observed in $[(C_4H_9)_4N]C_{43}$, and only this TAAGIC showed no solvent co-intercalation. The larger TAA cations form bilayer structures with significant DMSO co-intercalation, e.g. $[(C_7H_{15})_4N{\cdot}1.4DMSO]C_{63}$ or $[(C_{18}H_{37})(CH_3)_3N{\cdot}1.6DMSO]C_{60}$. Attempts to exchange TAA cations smaller than $(C_4H_9)_4N^+$ resulted only in high-stage GICs or graphite.

Earlier studies on the intercalation of TAA cations into graphite employed electrochemical reduction in organic electrolytes. Besenhard et al.[19] reported a dull-black, stage-1 GIC with $\Delta d = 1.25$ nm and approximate composition $[(CH_3)_4N{\cdot}6.0DMSO]C_{24}$ by the reduction of graphite in $(CH_3)_4NCl$/DMSO. The product was highly air sensitive and found to partially decompose during characterization. *Simonet*[20] reported the reversible intercalation/deintercalation of TAA cations by cyclic voltammetry on graphite in DMF-based electrolytes containing TAA cations. A galvanostatic charge plot showed the stepwise formation of $[(CH_3)_4N]C_x$, x = 96, 24, and 12. Zheng et al.[21] reported a new X-ray diffraction peak at 23.5° 2θ (d = 0.378 nm) after reducing graphite at different potentials in an ionic liquid electrolyte containing $(CH_3)_3(C_6H_{13})N^+$, suggesting the formation of a new TAAGIC at 0.7 V vs. Li/Li^+. The appearance and disappearance of this single peak during cyclic voltammetry suggested reversible intercalation/de-intercalation of the asymmetric TAA cation.

We are not aware of the electrochemical preparation, isolation, and characterization of any stable TAAGICs to date. In this work, we will describe a series of stable TAAGICs obtained by reduction in DMSO-based electrolytes. The products obtained are isolated and then characterized by X-ray diffraction, and thermogravimetric and elemental analyzes. In addition, the electrochemical reactions are evaluated using cyclic voltammetry.

Experimental

TIMREX SLP50 Graphite powder (TIMCAL America Inc., average particle diameter 50 μm) and all tetra-n-alkylammonium bromide (TAABr) salts with a purity >98% were used as received. The abbreviation TnA will be used for these symmetric cations, where n is the number of carbons per alkyl group, thus $(C_4H_9)_4N^+$ will be listed as T4A. DMSO (AR grade, 99.9%) and acetonitrile (HPLC grade, 99.9%) were dried over a 4 Å molecular sieve prior to use.

Galvanostatic reductions were performed in a two-compartment cell with a fritted glass separator, and were maintained under an inert atmosphere at ambient temperature. Working electrodes were prepared by painting a cyclohexane slurry containing graphite powder (20–25 mg) and 5 wt% polymer binder (EPDM) onto a stainless steel (SS) mesh flag (geometric area ∼1 cm^2). Coated electrodes were dried at 50°C. Counter and reference electrodes were SS mesh and wire. Repeated tests on the SS wire reference in the same electrolytes, both as prepared and after the reduction reaction, returned a potential of −0.03(1) V vs. SCE, and potentials reported below have been converted to V vs. SCE. Electrolyte solutions were 0.1 M TAABr in DMSO, except for T1ABr/DMSO which was found to saturate at a lower concentration. Graphite electrodes were reduced at a current density of 3.3 mA/g for 22 h. If the graphite reduction is fully efficient, the applied charge corresponds to a negative charge on graphene sheets of $x = 32$ in C_x^-. From previous results on the chemical intercalation of TAA cations, this is a significantly higher charge than required to form the stage-1 products.[17] Reductions for longer times were also tried in some cases, with no change in the products obtained. Following reduction, the working electrodes were immediately removed from the cell, rinsed briefly with 3–4 mL of acetonitrile, and then dried overnight under vacuum. Cyclic voltammetry was conducted at 1.0 mV/s, from 0 to −2.5 V vs. SCE, for one or more cycles. Electrode

[z]E-mail: Michael.Lerner@oregonstate.edu

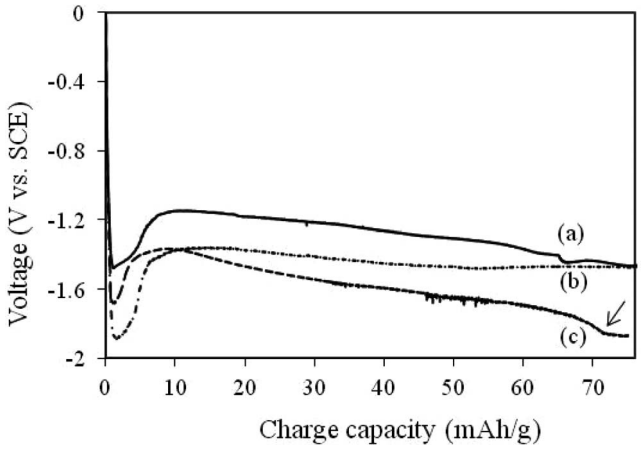

Figure 1. Galvanostatic potential-charge curves for graphite in (a) *sat*. T1ABr/DMSO, (b) 0.1 M T5ABr/DMSO and (c) 0.1 M T7ABr/DMSO electrolytes.

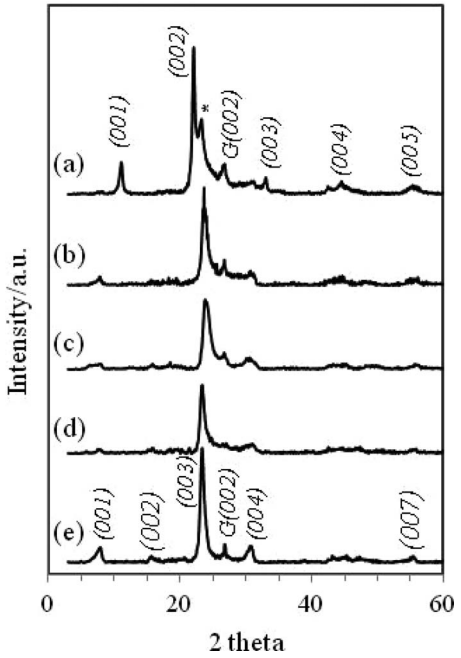

Figure 2. PXRD patterns of products obtained after galvanostatic reduction in 0.1 M (a) T4ABr/DMSO, (b) T5ABr/DMSO, (c) T6ABr/DMSO, (d) T7ABr/DMSO and (e) T8ABr/DMSO. The (*00l*) indexes all refer to stage-1 GIC products. The starred peak corresponds to an impurity phase (see text). *G*(*002*) denotes unreacted graphite.

preparation was similar to that described above but utilized ~2 mg of graphite on a 9 mm^2 SS flag.

Powder X-ray diffraction (PXRD) studies used a Rigaku Miniflex II diffractometer with Ni-filtered Cu K_α radiation. PXRD data were collected at 5°/min from 3° to 60° 2θ. Only (*00l*) reflections were indexed in the obtained PXRD patterns due to preferred orientation in the samples. The relationship between the gallery expansion (Δd), repeat distance along the c-direction (I_c), and the GIC stage number (n) is $I_c = \Delta d + 0.335n$, where 0.335 nm corresponds to the thickness of a single graphene sheet. Thermal analyzes used a Shimadzu TGA-50 thermogravimetric analyzer (TGA) under flowing Ar/O_2 (20 mL/min) at a heating rate of 10°C/min from ambient to 800°C. Sulfur elemental analyzes were performed by Micro-Analysis, Inc. (Wilmington, DE).

Results and Discussion

Three representative potential-charge curves are shown in Figs. 1a–1c. For all these curves, a sharp potential drop occurs at the outset, followed by a voltage increase and then a long, negatively-sloping plateau. A similar voltage decrease and recovery feature has been observed at the initial stage of electrode reduction for a range of chemistries, and is sometimes termed the "voltage delay".[22–24] The feature is generally ascribed to the formation of a passivation layer at the electrode surface. The appearance, voltage profile, and duration of the voltage delays depend on several factors including the electrode and electrolyte chemistry. In Fig. 1, the charge associated with these voltage delays is seen to be 5–10 mAh/g. For comparison, the formation of a passivation layer on graphite anodes in Li-ion batteries, known as the solid electrolyte interface, requires ~20–60 mAh/g.[25–27] After the surface passivation and voltage recovery, a subsequent intercalation reaction occurs with a gradually decreasing potential. No distinct potential steps are observed to indicate staging transitions; although a broad potential step was noted at 60–70 mAh/g for many cells (see arrow in Fig. 1). The absence or broadening of potential steps is likely associated with a relatively slow intercalation rate into the electrode bulk, resulting in a heterogeneous intercalate distribution and the formation and maintenance of a stage-1 TAAGIC at the electrode surface at the applied current density. Lower current densities were tested, but always resulted in high-stage GIC products due to the inefficiency of the overall reduction reaction.

Figure 2 shows PXRD data for the obtained TAAGICs, and derived structural data are summarized in Table I. With the larger TAA cations (Figs. 2b–2e), the reactions generate stage-1 products with $\Delta d = 0.81$ nm; all these patterns show the same structure and (*00l*) peak indexes, as indicated above Fig. 2e. The stage and gallery dimensions correspond to those obtained for the chemically-derived TAAGICs reported previously.[17] These gallery dimensions require sterically that the TAA cations are present in a highly-flattened conformation as shown in Fig. 3. T4AGIC (Fig. 2a) alone forms monolayers, with $\Delta d = 0.48$ nm, again in agreement with the chemically-derived TAAGICs. The starred peak at 23.4° 2θ in Fig. 2a might either be ascribed to a stage-2 monolayer phase or a stage-1 bilayer phase, in both cases the strongest reflection is (*003*), with a calculated position

Table I. The structural and compositional data for obtained TAAGICs.

Product	Stage	Δd_i (nm)	Intercalate arrangement	Total intercalate (mass pct)	Composition	Packing fraction
T4AGIC	1[a]	0.48	monolayer	36.5	$[(C_4H_9)_4N]C_{37} \cdot 0.1$DMSO	0.67
T5AGIC	1	0.81	bilayer	40.9	$[(C_5H_{11})_4N]C_{47} \cdot 0.7$DMSO	0.42
T6AGIC	1	0.81	bilayer	41.0	$[(C_6H_{13})_4N]C_{56} \cdot 0.8$DMSO	0.42
T7AGIC	1	0.82	bilayer	47.4	$[(C_7H_{15})_4N]C_{54} \cdot 1.2$DMSO	0.51
T8AGIC	1	0.81	bilayer	49.3	$[(C_8H_{17})_4N]C_{56} \cdot 1.2$DMSO	0.56

[a]impurity ascribed to bilayer phase.

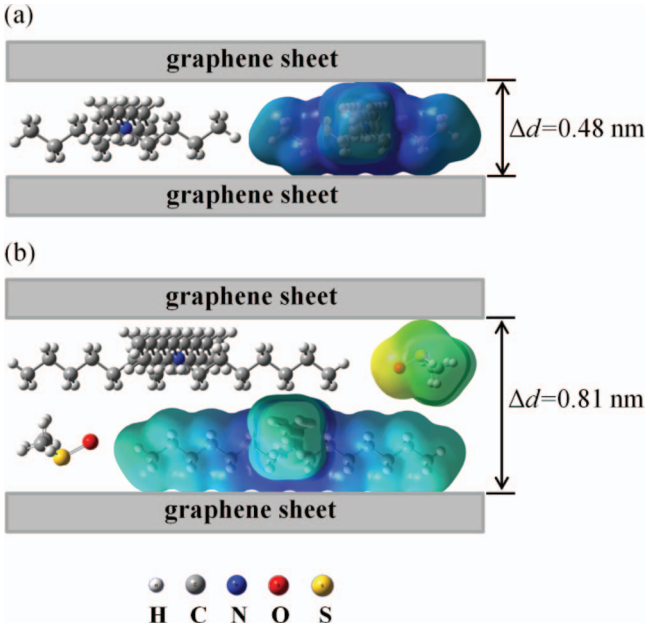

Figure 3. Schematic of intercalate conformations for (a) monolayer T4AGIC and (b) bilayer T7AGIC, including the DMSO co-intercalate for the bilayer phase. Both ball-and-stick (left) and space-filling representations (right) of the intercalates are shown.

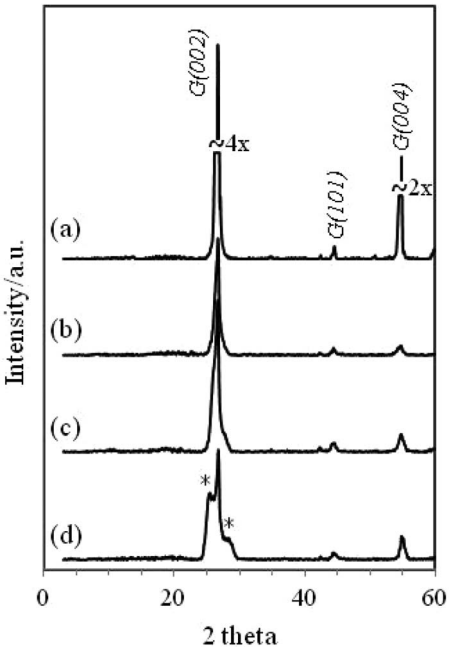

Figure 4. PXRD patterns of (a) pristine graphite, and after galvanostatic reduction in (b) *sat*. T1ABr/DMSO, (c) 0.1 M T2ABr/DMSO and (d) 0.1 M T3ABr/DMSO. *G*(*hkl*) denotes unreacted graphite reflections, and the starred peaks are from a high-stage GIC.

of 23.2 or 23.3° 2θ, for these respective alternatives. Given the compositional data analysis, described below, the assignment of this impurity phase as a stage-1 bilayer is more reasonable. Additionally, a small *G*(*002*) peak from unreacted graphite is observed for all samples.

As shown in Fig. 4, it is notable that TAA cations smaller than T4A did not generate low-stage GICs. This was also observed for the chemical exchange reactions, and seems at first counter-intuitive. Smaller cations might be expected to show higher diffusion rates into graphene galleries and therefore more readily generate GICs. In Fig. 4, the T1A and T2A cations show only a broadened graphitic reflection, whereas T3A generates a high-stage GIC along with graphite. The data and trend suggest that, as was observed earlier by Besenhard et al.,[19] a reaction does occur, GICs with the smaller TAA cations do form, but they are highly unstable and rapidly oxidize back to graphite, either in situ or during product workup.

We propose a passivation model to explain the increase in TAAGIC stability with increasing TAA size. TAA cations are known to generate alkyl radicals upon reductive decomposition at the potentials applied in these experiments,[28–30] according to:

$$(C_7H_{15})_4N^+ + e^- \rightarrow (C_7H_{15})_3N + C_7H_{15}\cdot \qquad [1]$$

The fate of these alkyl radicals depends on the species present and reaction conditions. In the aprotic and reductively-stable DMSO solvent, we propose that both small and large alkyl formed from TAA cations react to alkylate the graphene sheet edges:

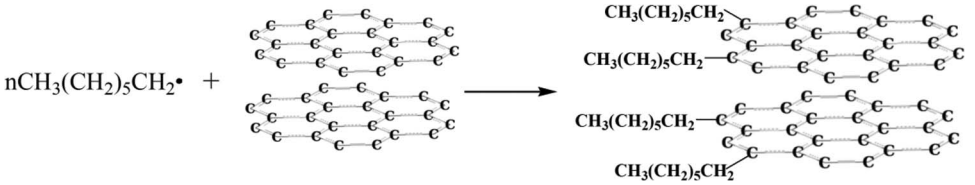

[2]

The exact nature of the surface chemistry during this reaction is not currently understood, and may be complex, however, the significant point for this model is that surface alkylation results. Then, only the longer surface alkyl groups can combine to form an effective passivation layer that stabilizes and permits isolation of a stable TAAGIC.

In Li-ion batteries, decomposition of the organic/Li salt electrolyte results in the formation of a protective solid electrolyte interphase (SEI) layer on the graphite surface. The insoluble SEI layer is about 20 nm thick, appears to consist predominantly of Li_2CO_3 and LiF, and permits rapid transfer of desolvated Li^+ ions.[31] Our proposed surface layer from TAA decomposition is likely to be thinner and more flexible, and, interestingly, permits the rapid transport of large TAA cations. This surface passivation and transport will be further described in a subsequent publication.

The TGA mass losses of selected TAAGICs are shown in Fig. 5. The unreacted electrodes (Fig. 5a) show a small loss at 300–450°C due to binder degradation, and the onset of graphite degradation is at 600°C. The binder content obtained by TGA (3.5 mass pct) is comparable to that used in the electrode formation slurry (5 pct). T4AGIC and T7AGIC (Figs. 5b, 5c) show multiple mass loss steps ascribed to thermolysis of the TAA cations at 120–580°C, polymer binder at 300–450°C, and graphite above 600°C. T7AGIC also exhibits a prominent mass loss below 120°C, ascribed to DMSO evaporation. The thermal decomposition of TAA cations in the TAAGICs begins at a lower temperature, and requires a wider temperature range, than the corresponding bromide salts. The decreased thermal stability of

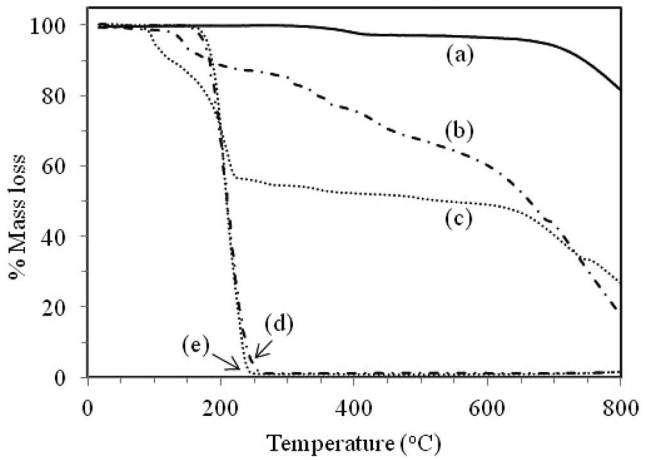

Figure 5. TGA plots for (a) graphite with EPDM binder, (b) T4AGIC, (c) T7AGIC, (d) T4ABr and (e) T7ABr.

TAA cations has been attributed to the catalytic effect of graphene sheets.[32,33]

After correcting for binder content, the TAAGIC compositions obtained by the above TGA assignments are shown in Table I. Compared with the $x = 43$ value obtained in the chemically-derived product, the T4AGIC with $x = 37$ has a relatively high intercalate content, consistent with an impurity bilayer phase (that will have a higher intercalate content) rather than an impurity stage-2 phase (that will be poorer in intercalate). Also, the T4AGIC product obtained does contain a small DMSO co-intercalate content, unlike the chemically-derived product. DMSO mass contents in T4AGIC and T7AGIC from TGA were calculated at 1.5 and 8.7 mass pct, respectively, consistent with sulfur elemental analyzes for these samples, which yielded 1.7 mass pct DMSO for T4AGIC and 9.8 mass pct DMSO for T7AGIC. Again, a bilayer impurity phase, but not a stage-2 phase, is more appropriate to explain the minor presence of DMSO.

Lattice enthalpies for GICs generally decrease for larger gallery expansions, and in the simplest electrostatic model might be expected to scale with $1/\Delta d$. However, bilayer galleries can be favored over monolayers when larger ion monolayers cannot compensate the host sheet charge densities. The formation of monolayers vs. multilayers for different intercalates is well-known for other charged host structures.[34–36] In order to further evaluate these effects, the packing fraction of intercalate galleries was calculated for the obtained TAAGICs. This fraction was determined by taking the ratio of the intercalate volume, estimated using the VABC (Atomic and Bond Contributions of van der Waals volume) method,[37] to the gallery volume, obtained from the observed TAAGIC gallery expansions, product compositions, and a surface area for graphene sheets of 0.0261 nm^2/C atom. The derived packing fractions are indicated in Table I, and show that the monolayer arrangement (with some bilayer impurity phase) to be the most densely packed gallery. The maximum achievable packing fraction from geometric considerations is not apparent for these irregularly-shaped, flattened TAA cations, but the transition to an exclusively bilayer arrangement is consistent with the greater spatial requirements to accommodate the larger TAA cations. Additionally, it is notable that the x values obtained for the bilayer GICs, from 47 to 56, indicate that unusually-low sheet charge densities are obtained for stage-1 GICs with these large TAA cation intercalates. Since lattice enthalpies also depend on sheet charge densities, and the chemical and electrochemical properties, including delamination, depend on lattice enthalpies, the ability to control sheet charge densities on GICs by selection of intercalate cation size could be a significant step toward producing GICs with novel properties.

The electrochemical behavior of graphite electrodes in TAABr/DMSO electrolytes was also investigated by cyclic voltammetry. As shown in Figs. 6a, 6d, the electrolytes themselves are stable to about −2.3 to −2.6 V on a Pt foil electrode. Previous reports

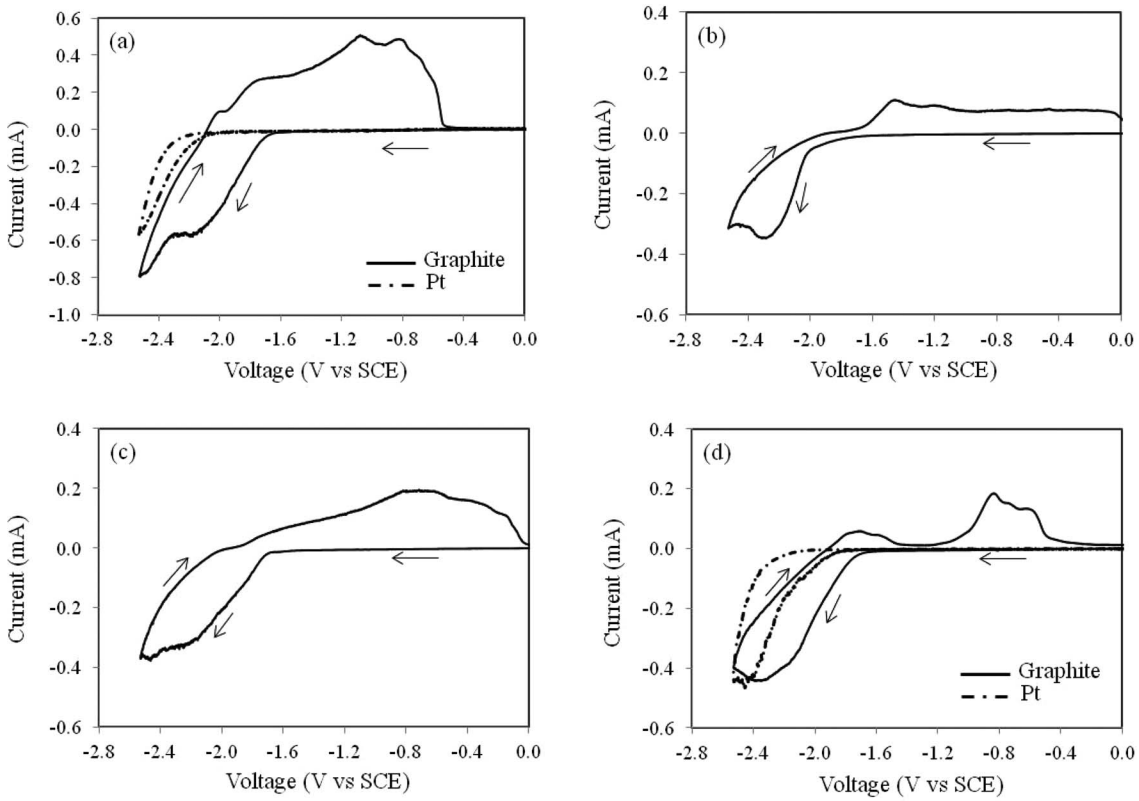

Figure 6. Cyclic voltammograms of graphite in 0.1 M (a) T2ABr/DMSO, (b) T3ABr/DMSO, (c) T5ABr/DMSO and (d) T7ABr/DMSO at a scan rate of 1 mV/s.

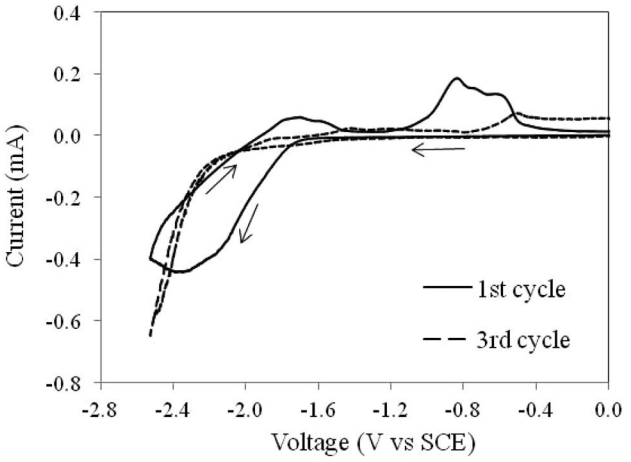

Figure 7. Cyclic voltammetry of graphite in 0.1 M T7ABr/DMSO at a scan rate of 1 mV/s.

indicate the irreversible reduction of T2A and T7A at similar potentials to yield the corresponding amines.[28] Our evaluation of a 0.1 M $LiN(SO_2CF_3)_2$/DMSO electrolyte under similar scans from 0 to −2.8 V shows no cathodic decomposition, demonstrating the stability of the DMSO solvent at low potentials (data not shown).

Graphite electrodes in 0.1 M TAABr/DMSO electrolytes exhibit a new broad cathodic reaction with onset at −1.6 V and current peak near −2.2 V. This cathodic feature is ascribed to reductive TAA intercalation, and the very broad and sometimes multiple anodic peaks from −2.0 to −0.5 V in the case of T2A, are ascribed generally as oxidative de-intercalation of the GIC. The round-trip coulombic efficiency for the first voltammetric cycle was 96% for T2A; this efficiency decreases with increased cation size down to 26% for T7A. The lower chemical reversibility for larger cations suggests a diffusion-limited de-intercalation process. The graphite sheet charge density, expressed as x in $C_x^{-\cdot}$ is 35 for T2A as compared with 37 for T4AGIC (Table I), indicating that a stage-1 T2AGIC was formed in situ during cyclic voltammetry. As described above, this T2AGIC is unstable and cannot be isolated after galvanostatic reduction.

Since galvanostatic methods show that TAA cations smaller than T4A do not form stable low-stage GICs, whereas cyclic voltammetry shows the characteristic features of intercalation/de-intercalation for these cations, and even suggests more rapid diffusion and more efficient processes for the smaller TAA cations. Putting these results together we can conclude that the smaller TAAs readily form GICs but they are unstable and rapidly decompose back to graphite or high-stage GICs, as noted by Besenhard et al. previously,[19] and that the stability of the larger TAAGICs is consistent with the formation of a more effective passivation layer as proposed above.

Figure 7 displays the first and third voltammetric cycles for graphite in 0.1 M T7ABr/DMSO. The first cycle exhibits reversible electrochemical intercalation/de-intercalation along with the irreversible decomposition of T7A cations at lower potential. The charges associated with cathodic and anodic scans were 0.32 and 0.082 C, respectively. The ratio suggests that only a minor fraction of the TAA intercalates are released from the galleries after intercalation. This indicates the slow diffusion of DMSO-solvated T7A cations within the galleries. The second cycle (not shown) shows lower currents with greater separation of cathodic and anodic peak potentials. For the third cycle (shown), this trend continues, with the cathodic sweep dominated by the TAA reduction rather than intercalation. Slow TAA diffusion results in dampened intercalation/de-intercalation on cycling even at the low sweep rate employed. Large TAA cations would not appear to be interesting as reversible insertion/de-insertion guests, such as for use directly in rechargeable electrodes. On the other hand, these cations might be introduced and retained within graphene galleries, and thereby modify the gallery chemistry and structure for accommodation of other guests.

Conclusions

A series of TAAGICs has been prepared and characterized for the first time by cathodic reduction in DMSO-based electrolytes. The monolayer or bilayer TAA galleries contain an unusual flattened conformation for the intercalate cations. Co-intercalation of the DMSO occurs significantly for the bilayer arrangement. The observed gallery expansions and compositions of these electrochemical products closely agree with those obtained for chemically-derived TAAGICs. TAA cations smaller than T4A do not form stable TAAGICs, although cyclic voltammetry indicates that intercalation does occur. A model is proposed with formation of a surface passivation layer by the alkylation of graphene edge surfaces that is consistent with the known reduction chemistry of TAA cations and the greater stability of the GICs containing larger TAA cations.

References

1. M. S. Dresselhaus and G. Dresselhaus, *Adv. Phys.*, **51**, 1 (2002).
2. L. B. Ebert, *Annu. Rev. Mater. Sci.*, **6**, 181 (1976).
3. W. C. Forsman, T. Dziemianowicz, K. Leong, and D. Carl, *Synth. Met.*, **5**, 77 (1983).
4. T. Maluangnont, W. Sirisaksoontorn, and M. M. Lerner, *Carbon*, **50**, 597 (2012).
5. Y. Mizutani, T. Abe, K. Ikeda, E. Ihara, M. Asano, T. Harada, M. Inaba, and Z. Ogumi, *Carbon*, **35**, 61 (1997).
6. T. Abe, H. Fukuda, Y. Iriyama, and Z. Ogumi, *J. Electrochem. Soc.*, **151**, A1120 (2004).
7. J. O. Besenhard, *Carbon*, **14**, 111 (1976).
8. T. Enoki, M. Suzuki, and M. Endo, *Graphite Intercalation Compounds and Applications*, Oxford University Press, New York (2003).
9. J. M. Thomas, G. R. Millward, R. F. Schlögl, and H. P. Boehm, *Mater. Res. Bull.*, **15**, 671 (1980).
10. V. A. Sethuraman, L. J. Hardwick, V. Srinivasan, and R. J. Kostecki, *J. Power Sources*, **195**, 3655 (2010).
11. Z. Ogumi and M. Inaba, *Bull. Chem. Soc. Jpn.*, **71**, 521 (1998).
12. S. Fukada, Y. Shintani, M. Shimomura, F. Tahara, and R. Yagi, *Jpn. J. Appl. Phys.*, **51**, 085101 (2012).
13. A. Mukherjee, J. Kang, O. Kuznetsov, Y. Sun, R. Thaner, A. S. Bratt, J. R. Lomeda, K. F. Kelly, and W. E. Billups, *Chem. Mater.*, **23**, 9 (2011).
14. Q. T. Truong, P. Pokharel, G. S. Song, and D. S. Lee, *J. Nanosci. Nanotechnol.*, **12**, 4305 (2012).
15. T. Wei, Z. Fan, G. Luo, C. Zheng, and D. Xie, *Carbon*, **47**, 337 (2009).
16. M. Toyoda and M. Inagaki, *Carbon*, **38**, 199 (2000).
17. W. Sirisaksoontorn and M. M. Lerner, *Inorg. Chem.*, **52**, 7139 (2013).
18. W. Sirisaksoontorn, A. A. Adenuga, V. T. Remcho, and M. M. Lerner, *J. Am. Chem. Soc.*, **133**, 12436 (2011).
19. J. O. Besenhard, H. Möhwald, and J. J. Nickl, *Carbon*, **18**, 399 (1980).
20. J. Simonet, *J. Electrochem. Commun.*, **30**, 17 (2013).
21. H. Zheng, K. Jiang, T. Abe, and Z. Ogumi, *Carbon*, **44**, 203 (2006).
22. Y. Ko and C. T. Lee, *J. Ind. Eng. Chem.*, **18**, 726 (2012).
23. J. O. Besenhard, E. Theodoridou, H. Möhwald, and J. J. Nickl, *Synth. Met.*, **4**, 211 (1982).
24. A. Leef and A. Gilmour, *J. Appl. Electrochem.*, **9**, 663 (1979).
25. M. C. Smart, B. V. Ratnakumar, S. Surampudi, Y. Wang, X. Zhang, S. G. Greenbaum, A. Hightower, C. C. Ahn, and B. Fultz, *J. Electrochem. Soc.*, **146**, 3963 (1999).
26. C. Yuqin, L. Hong, W. Lie, and L. Tianhong, *J. Power Sources*, **68**, 187 (1997).
27. Y. Matsumura, S. Wang, and J. Mondori, *J. Electrochem. Soc.*, **142**, 2914 (1995).
28. C. E. Dahm and D. G. Peters, *J. Electroanal. Chem.*, **402**, 91 (1996).
29. G. Eggert and J. Heitbaum, *Electrochim. Acta*, **31**, 1443 (1986).
30. J. S. Mayell and A. J. Bard, *J. Am. Chem. Soc.*, **85**, 421 (1963).
31. K. Xu and A. Cresce, *J. Mater. Res.*, **27**, 2327 (2012).
32. N. Muradov, F. Smith, and A. T-Raissi, *Catal. Today*, **102–103**, 225 (2005).
33. R. Q. Sun, L. B. Sun, Y. Chun, and Q. H. Xu, *Carbon*, **46**, 1757 (2008).
34. L. Mercier and C. Detellier, *Clays Clay Miner.*, **42**, 71 (1994).
35. Y. Chun, G. Sheng, and S. A. Boyd, *Clays Clay Miner.*, **51**, 415 (2003).
36. Z. Li and W. T. Jiang, *Thermochim. Acta*, **483**, 58 (2009).
37. Y. H. Zhao, M. H. Abraham, and A. M. Zissimos, *J. Org. Chem.*, **68**, 7368 (2003).